Tianjin Daxue Xuebao (Ziran Kexue yu Gongcheng Jishu Ban)/
Journal of Tianjin University Science and Technology
ISSN (Online):0493-2137
E-Publication: Online Open Access
Vol: 59 Issue: 04:2026
DOI: 10.5281/zenodo.19495381

FAGAS-NET: BONE SARCOMA BOUNDARY DELINEATION USING A FRACTAL–ADAPTIVE GRAPH ATTENTION SEGMENTATION NETWORK

P. J. ADIT
Research Scholar, Department of Computer Science, Dr.M.G.R. Educational and Research Institute, Chennai, Tamil Nadu, India. Email: pjadit1802@gmail.com

Dr. C. PRIYA
Professor and Research Supervisor, Faculty of Computer Applications, Dr.M.G.R. Educational and Research Institute, Chennai, Tamil Nadu, India. Email:drcpriya.research@gmail.com

Abstract

Bone sarcoma is a high grade underlying bone malignancy in teenagers and young adults, where the proper delineation of tumor boundary is imperative in the early diagnosis and treatment planning. The common drawback of existing segmentation techniques is that cannot handle heterogeneous tumor textures, low contrast and lesion margins, resulting in uneven clinical results. The research proposed the Fractal-Adaptive Graph Attention Segmentation Network (FAGAS-Net) and which incorporates multi-step denoising, feature improvement, and graph attention. The first step is to normalized the image and enhance its contrast in order to equalize the intensity and enhance the visibility of the tumor region. Multi-scale convoluting and fractal-based feature enhancement are then used which detects not only the global structural features but also fine tumor textures and channel attention identifies discriminative tumor regions. The improved features are used with adaptive graph attention to learn the spatial dependencies which results in a probability map, which is threshold to give the final binary segmentation mask. It has been experimentally evaluated that FAGAS-Net has better performance than other available ones with Dice Similarity Coefficient of 0.978, which represents correct and reliable results in delineating tumors. The solution creates a potent instrument to analyze bone sarcoma and forms a basis of future interconnection with multimodal imaging and processes.

Keywords: Attention Mechanism, Bone Tumor Segmentation, Fractal Feature Enhancement, Graph Neural Network, Histopathological Imaging, Bone Sarcoma.

1. INTRODUCTION

Bone sarcoma is a primary malignant bone tumors, is a clinically challenging tumor because of its high rate of progression and difficult morphology. Early and precise image analysis of bone sarcoma plays a vital role in enhancing the prognosis of patients and determining the best treatment approach [1].

Bone sarcoma is a severe primary bone tumor that mostly affects adolescents and young adults, with early delineation of tumor boundaries being very important in the early diagnosis and formulation of effective treatment plans. Recent deep learning methods such as stacked sparse autoencoders, convolutional neural networks, and hybrid multilayer perceptors models have enhanced tumor detection and classification [2], but fail with heterogeneous tumor textures [3] and low-contrast areas [4].

Tianjin Daxue Xuebao (Ziran Kexue yu Gongcheng Jishu Ban)/
Journal of Tianjin University Science and Technology
ISSN (Online):0493-2137
E-Publication: Online Open Access
Vol: 59 Issue: 04:2026
DOI: 10.5281/zenodo.19495381

Ensemble learning and swarm-optimized deep learning systems have tried to improve robustness [5] and pretrained models and explainable AI frameworks further improve predictive accuracy [6], but gated recurrent unit-based optimization models propose that accurate segmentation is still necessary [7]. Altered ensemble classifiers [8] and honey badger optimization with transfer learning [9] have been used to do better bone sarcoma classification; most models are detection-based whereas few are pixel-based delineation [10]. IoMT-enabled transfer learning systems [11] and variability-friendly training systems [12] are solutions to data heterogeneity, but segmentation in low-contrast or irregular tumor areas [13], transfer learning piping to detect tuberculosis in chest X-ray images [14], and bilateral dilated CNN to segment cardiac images [15] show that enhanced attention-controlled segmentation methods are needed to effectively delineate tumor edges in multifaceted images.

This is inspired by the fact that the existing approaches of segmentation of bone sarcoma are restricted due to their vulnerability to deal with the heterogeneous texture of tumors, low contrast images and disordered boundary structure of the histopathology images. Proper boundary delineation is important to be able to diagnose and plan the treatment accurately, but most deep learning systems are detection-based and not pixel-based.

In this research, fill this gap by developing a new framework, FAGAS-Net, a hybrid framework, which combines an improved denoising, fractal-based multi-scale feature enhancement, and adaptive graph attention in the context of robust tumor segmentation.

The most important contribution is that it is effective in capturing both the global structural context and fine-grained tumor morphology at the same time maintaining fitness in boundary precision.

Organization: The segmentation of bone sarcoma is presented in this research; Section 1 is a introduction and the background study in Section 2. Section 3 describes Enhanced Eformer denoising and FAGAS-Net segmentation framework and dataset details, and then Section 4 gives the results and discussion.

Lastly, Section 5 is the conclusion of the research and it identifies contributions, limitations and future directions of bone sarcoma image analysis.

2. BACKGROUND STUDY

Georgeanu et al. (2022) [16] proposed a deep learning-based MRI image analysis system of malignant bone tumor diagnosis by CNN architecture. Though this research achieved good feature learning which enhanced classification accuracy, it did not include fine-grained boundary segmentation and robustness analysis across heterogeneous datasets which restricted its generalizability despite the better diagnostic performance.

Breden et al. (2023) [17] created a deep-learning-based bone tumor detection model around the knee based on pediatric X-ray images to determine bone tumors using CNN-based classification models. The method despite the fact that high detection sensitivity

Tianjin Daxue Xuebao (Ziran Kexue yu Gongcheng Jishu Ban)/
Journal of Tianjin University Science and Technology
ISSN (Online):0493-2137
E-Publication: Online Open Access
Vol: 59 Issue: 04:2026
DOI: 10.5281/zenodo.19495381

was attained was interested in rough detection and not fine tumor delineation and did not consider the noise and small-lesion ambiguity.

Kim et al. (2021) [18] used convolutional neural networks on PET image centers to predict the response to chemotherapy in the cases of bone sarcoma. The method showed good predictive capability, but used inputs in region level without segmentation editing and was not flexible to image noise variability.

Mămuleanu et al. (2022) [19] used deep learning segmentation architectures to automatically outline lesions in encoder-decoder CNNs. Although the region was accurately extracted, adaptive attention or multi-scale contextual learning was not incorporated in the study, which curtailed boundary accuracy in multifaceted lesion shapes.

According to Zhao et al. (2023) [20], a multimodal CNN feature fusion predictive model of PET/MR imaging was developed, based on deep learning. Although it improved the performance of prediction, the uncertainty modeling and generative denoising were not implemented to improve features reliability.

Pati et al. (2023) [21] proposed a transfer deep learning architecture (CanDiag), which is based on the use of fog to execute architecture-based cancer diagnosis using pretrained CNN models. In spite of the fact that the computational efficiency was enhanced, the model did not possess high-level segmentation intelligence and resistance to structural variations of complex images.

Chen et al. (2025) [22] improved the YOLOv11 with large kernel attention and multi-scale fusion to identify small and multi-lesion bone tumors in radiographs. This approach was better in detection accuracy, but it was still detection-based and did not consider boundary segmentation and noise reduction on a pixel-level.

Karabağ et al. (2023) [23], semantic segmentation using the deep CNNs structure was investigated under varying training data, shape, and ground truth prerequisites. The research revealed that there were robustness issues during the treatment of variability of shapes but did not propose any adaptive or graphical processes to solve the issue of boundary inconsistency.

Wang et al. (2022) [24] introduced an auxiliary segmentation approach combining denoising and local enhancement prior to CNN-based segmentation of bone sarcoma MRI images. Although denoising improved segmentation clarity, the approach relied on existing enhancement rather than probabilistic diffusion-based noise modeling.

Sabir et al. (2022) [25] implemented a ResU-Net architecture for tumor segmentation using CT images, leveraging residual learning for improved convergence. Despite accurate segmentation results, the model lacked adaptive attention and struggled with fine boundary preservation in heterogeneous image conditions.

Tianjin Daxue Xuebao (Ziran Kexue yu Gongcheng Jishu Ban)/
Journal of Tianjin University Science and Technology
ISSN (Online):0493-2137
E-Publication: Online Open Access
Vol: 59 Issue: 04:2026
DOI: 10.5281/zenodo.19495381

Table 1: Comparison table of segmentation and bone sarcoma detection models using deep learning algorithms

Authors (Year)	Concept / Objective	Methods Used	Research Gap	Limitations	Key Results
Wang *et al.* (2025) [26]	Bone tumor segmentation and 3D visualization using mixed reality	DCU-Net-based deep learning segmentation integrated with mixed reality infrastructure	Lacks histopathological image-based validation	High computational cost and hardware dependency	Achieved accurate bone tumor segmentation and enhanced 3D visualization
Brunese *et al.* (2025) [27]	Explainable deep learning for medical image segmentation	U-Net with explainability and robustness enhancement techniques	Focused on liver images, not bone tumors	Limited cross-dataset generalization	Improved segmentation accuracy with better model interpretability
Della Reasa Valiaveetil (2025) [28]	Automated leukemia detection	SegNet combined with Faster R-CNN	Not designed for solid tumor or bone segmentation	Classification-oriented, no boundary refinement	Achieved reliable leukemia detection performance
Zhou *et al.* (2025) [29]	Intelligent image layout segmentation	Enhanced DeepLabV3+ with multi-scale feature optimization	Applied to document images, not medical imaging	Domain-specific feature design	Superior segmentation and classification accuracy
Lu *et al.* (2025) [30]	Pulmonary embolism detection in CT angiography	AI-enhanced deep learning framework with CNN-based feature extraction	Disease- and modality-specific	No segmentation focus on tumors	High detection accuracy in CT angiography images

Table 1 is a summary of recent studies in the field of deep learning-based segmentation and detection applicable to the medical imaging sphere. Despite the good performance in the areas, the majority of these methods are not directly relevant to the histopathological bone tumor segmentation and as such, a specific framework like the FAGAS-Net is required.

3. Proposed Methodology

The research provides a combined system of bone sarcoma segmentation, which involves Enhanced Eformer for denoising and FAGAS-Net for segmentation. The method enhances image, maintains tumor structures and precisely delineates tumor margins that makes reliable diagnosis and clinical interpretation.

Figure 1 demonstrates the integration of Enhanced Eformer where the tumor-biased image-denoising process of forward diffusion and noise prediction is realized and followed by the FAGAS-Net framework that performs segmentation through fractal-adaptive graph attention. The outcomes of the workflow are the generation of tumor masks, overlay segmentation, and contour mapping in order to tumor areas and boundaries clearly.

Tianjin Daxue Xuebao (Ziran Kexue yu Gongcheng Jishu Ban)/
Journal of Tianjin University Science and Technology
ISSN (Online):0493-2137
E-Publication: Online Open Access
Vol: 59 Issue: 04:2026
DOI: 10.5281/zenodo.19495381

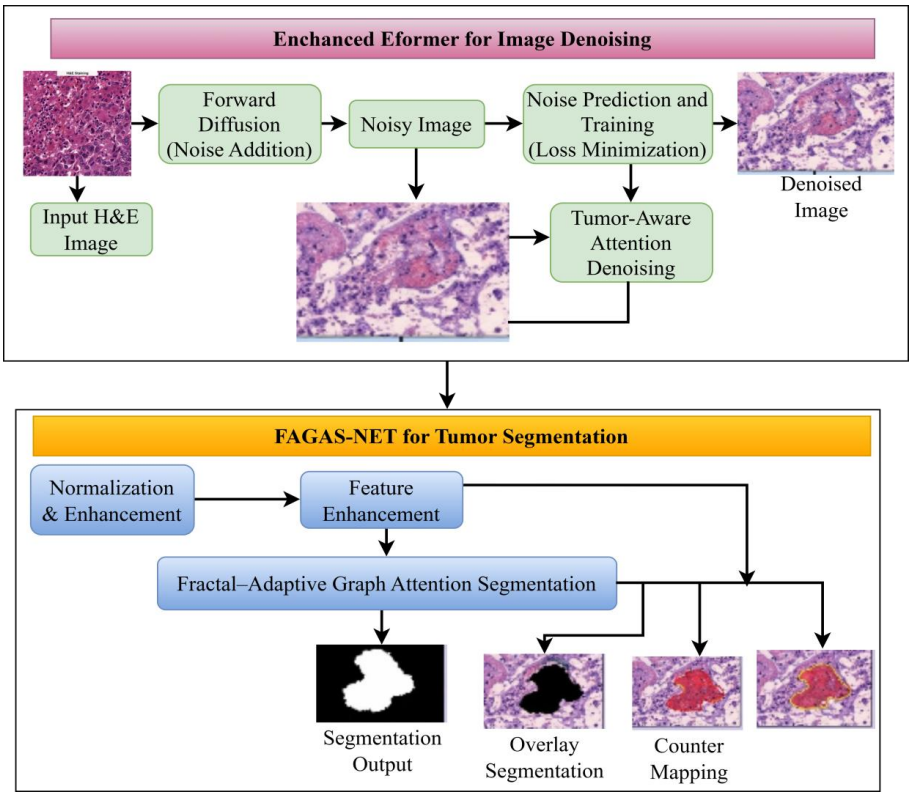

Figure 1: Workflow of Enhanced Eformer and FAGAS-Net to Bone tumor Segmentation

3.1 Dataset Information

The Bone sarcoma dataset that used is available on Kaggle https://www.kaggle.com/datasets/gauravupadhyay0312/bone sarcoma, and it includes histopathological images of bone tissue, usually stained with Hematoxylin and Eosin (H&E), which are used to train and test machine learning and deep learning algorithms to analyze tumors. These images are associated with various categories like non tumor tissue, viable tumor, and necrotic tumor, hence automated detection and classification processes in bone sarcoma studies detailing how the healthy and malignant bone mass would appear visually different. The dataset can be used in research that focuses on enhancing diagnostic accuracy and strength of AI models on actual clinical imaging datasets to assist researchers to design and test segmentation and classification models of bone cancer.

3.2 Enhanced Eformer Workflow for Bone Tumor Image Denoising

The research use the Edge Enhancement based Transformer for Medical Image Denoising (Eformer) [24] to enhance the quality of the bone tumor images by successfully denoising and retaining important structural features. The proposed solution builds upon the idea of the multi-stage diffusion approach whereby noisy input images are sequentially improved by using a series of denoising steps using a learned probabilistic

Tianjin Daxue Xuebao (Ziran Kexue yu Gongcheng Jishu Ban)/
Journal of Tianjin University Science and Technology
ISSN (Online):0493-2137
E-Publication: Online Open Access
Vol: 59 Issue: 04:2026
DOI: 10.5281/zenodo.19495381

model. Through the noise distribution modeling and learning to learn how to reverse the noise, the enhanced Eformer can restore fine-grained details in medical images, and it is essential to accurate diagnosis. The model applies attention mechanisms to concentrate on tumor regions whereby the model will keep the relevant anatomical structures and eliminate the irrelevant noise. Moreover, diffusion process is improved by adaptive noise scheduling and residual learning to speed up the convergence and increase the denoising performance. This algorithm is used to test bone tumor data, it shows significant improvements in image clarity and contrast relative to the exisiting denoising algorithms. Altogether, this approach provides an effective platform of work on bone tumor image improvement to facilitate downstream activities, such as the segmentation and classification.

$$q(x_{t-1}|x_t) = \mathcal{N}\left(x_t; \sqrt{1-\beta_t}x_{t-1}, \beta_t I\right) \qquad (1)$$

Equation 1 x_t Noise at time t, x_{t-1} Image at time $t-1$ (less noisy), β_t Noise schedule coefficient Noise to add at time t, I Identity matrix, is sampled by a Gaussian method $\mathcal{N}$, is resampled by a Gaussian method. Control the denoising model by training with noises the image at each step, gradually progressing in its degradation.

$$p\theta(x_{t-1}|x_t) = \mathcal{N}(x_{t-1}; \mu_\theta(x_t, t), \sum_\theta(x_t, t)) \qquad (2)$$

Equation 2 x_t Noisy image at time t, x_{t-1} Less-noisy image at time step $t-1$, $p\theta(x_{t-1}|x_t)$ Likelihood or probability of the neural network to reconstruct x_{t-1}, $\mathcal{N}(.;\mu,\Sigma)$ Gaussian distribution, with mean μ and covariance Σ, $\mu_\theta(x_t,t)$ Mean of the predicted image, x_{t-1}, at time t, $\sum_\theta(x_t,t)$ Variance of the predicted image, x_{t-1}, at time t. The equation recursively forecasts and eliminates noise on x_t to restore the original image x_0 with several timesteps.

$$L_{simple} = \mathbb{E}_{x_0 \in \sim \mathcal{N}(0,1),t}[\|\in -\in_0 (x_t, t)\|^2] \qquad (3)$$

Equation 3 L_{simple} The loss function which counts the amount to which the network is able to predict noise, $\mathbb{E}_{x_0,\in,t}[\cdot]$ Expected error on all images x_0, noise $\in$, and time steps t averages the error on the noise across the entire dataset, x_0 The original clean image with no noise, $\in \sim \mathcal{N}(0,1)$ True Gaussian noise added to the image in time step t, $\in_0 (x_t, t)$ Noise as predicted by the neural network at timestep t. The network is trained under minimizing the difference between the actual noise and the predicted noise, hence, can effectively denoise images in the reverse diffusion process.

$$x_0 = \frac{x_t - \sqrt{1-\alpha_t}\in\theta(x_t,t)}{\sqrt{\alpha_t}} \qquad (4)$$

Equation 4 x_0 Original clean image that are trying to reconstruct, x_t Noisy image at diffusion step t, $\in \theta(x_t,t)$ Noise, predicted by the neural network at step t, $\alpha_t = 1-\beta_t$ Scaling factor derived by the noise schedule β_t Predefined noise coefficient that controls the strength of the noise added at step t, It is the predicted noise subtracted from the noisy image x_t and rescaled to get the original clean image x_0.

$$\mu_\theta(x_t,t) = (1-\gamma)\mu_{global}(x_t,t) + \gamma\mu_{tumor}(x_t,t) \qquad (5)$$

Tianjin Daxue Xuebao (Ziran Kexue yu Gongcheng Jishu Ban)/
Journal of Tianjin University Science and Technology
ISSN (Online):0493-2137
E-Publication: Online Open Access
Vol: 59 Issue: 04:2026
DOI: 10.5281/zenodo.19495381

Equation 5 $\mu_\theta(x_t, t)$ Predicted denoised mean, x_t Noisy bone tumor image at time t, t Diffusion time step, $\mu_{global}(x_t, t)$ Predicted Denoised mean, $\mu_{tumor}(x_t, t)$ Predicted Denoised mean concentrated on tumor areas, gamma: $0 \leq \gamma \leq 1$. This equation is a dynamically adjusted image denoising image globally that uses an attention weight to increase the critical tumor information at the expense of the overall image quality.

3.3 Segmentation Using Fractal–Adaptive Graph Attention Segmentation Network (FAGAS-Net)

The algorithm presents a Fractal Adaptive Graph Attention Segmentation Network (FAGAS-Net) that tries to provide the correct localization of the bone tumor of the medical images. The framework uses systematic workflow that is Comprised of Normalization Enhancement, Feature Enhancement, and Segmentation whereby the last stage is segmentation that is the main aim. The denoising phases are predetermined with the quality of the image and discriminability of the features that should be utilized to be capable of supporting the process of segmentation. The algorithm can attract spatial dependencies, tumor properties based on adaptive learning and graph-based learning. It is a high localization of the tumor with clear delimiting boundaries in this monolithic structure.

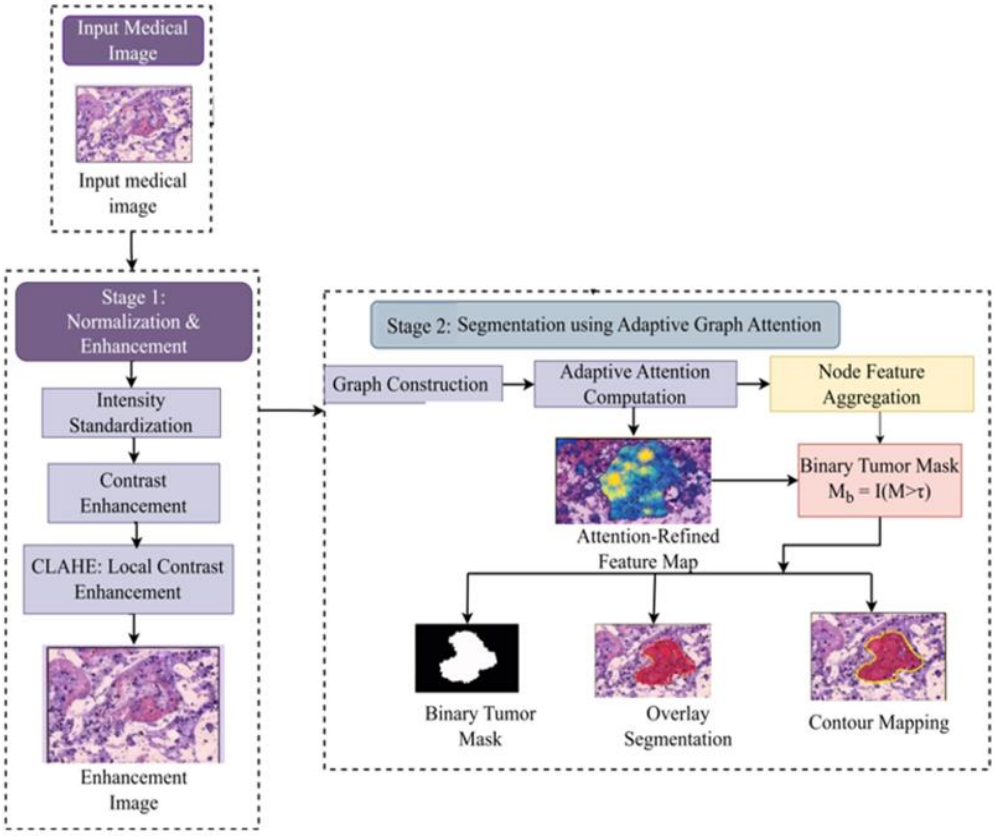

Figure 2: Workflow of the Prescribed FAGAS-Net Framework of Bone Tumor Segmentation

Tianjin Daxue Xuebao (Ziran Kexue yu Gongcheng Jishu Ban)/
Journal of Tianjin University Science and Technology
ISSN (Online):0493-2137
E-Publication: Online Open Access
Vol: 59 Issue: 04:2026
DOI: 10.5281/zenodo.19495381

Figure 2 illustrates the general process of the FAGAS-Net system, where image normalization and image enhancement are performed, followed by fractal-attention-based refinement of the features, and the segmentation can be achieved with the help of adaptive graph attention. The output of the operation is a binary tumor mask and overlay segmentation and contour mapping to accurately visualize the tumor areas and margins.

3.3.1. Normalization Enhancement

Normalization is the initial phase of denoising which prepares bone tumor images in a way that is successful in segmentation. The width of the contrast and the increase of contrast techniques used, the difference between purchases made due to noise and non-uniform acquisition conditions is reduced by the process of normalization. Normalization Adaptive normalization and histogram equalization normalize the pattern of pixel values and result in a better visual appearance of the difference between tumor and bone tissue. The step increases the contrast of low-contrast tumor regions and removes the background artifacts. As such, normalization provides stable and quality input to succeeding processing phases.

$$I_{norm} = \frac{I - \mu_I}{\sigma_I} \qquad (6)$$

Equation 6 Where I is the original input bone tumor image, μ_I mean pixel value of the image, σ_I standard deviation of pixel values and I_{norm} normalized image. The equation is used to normalize the pixel brightness to reduce the change in brightness and increase consistency of the image.

$$I_{enh} = \alpha \cdot I_{norm} + \beta \qquad (7)$$

Equation 7 α Contrast scaling factor, β Intensity shift parameter, I_{enh} Enhanced image. It enhances visual contrast thus rendering tumor areas easier to distinguish against surrounding tissue.

$$I_{mm} = \frac{I_{enh} - I_{min}}{I_{max} - I_{min}} \qquad (8)$$

Equation 8 I_{min}, I_{max} Minimal and maximal intensity, I_{mm} Minmax normalized image. Necessitates the conversion of the pixel values to the normal range of [0, 1] to allow the same training of the network.

$$I_{clahe} = CLAHE(I_{mm}) \qquad (9)$$

Equation 9 I_{clahe} Locally adaptive image, $CLAHE(\cdot)$ Contrast Limited Adaptive Histogram Equalization. Enhances the local contrast of low-intensity tumor regions and limits the noise amplification.

3.3.2. Feature Enhancement

The feature improvement intends to obtain discriminative representations that are required to obtain a suitable tumor boundary. The use of multi-scale convolutional and fractal based representations are being used in order to obtain the global and fine tumor texture patterns.

Tianjin Daxue Xuebao (Ziran Kexue yu Gongcheng Jishu Ban)/
Journal of Tianjin University Science and Technology
ISSN (Online):0493-2137
E-Publication: Online Open Access
Vol: 59 Issue: 04:2026
DOI: 10.5281/zenodo.19495381

The adaptive graph attention mechanisms have the capacity to attract attention to the spatially significant areas that enhance the tumor specific features and reduce the information of the background. This higher representation of features makes features sensitive to non-regular shapes of tumors. Consequently, context sensitive feature is transferred to the segmentation module that enables the localization to be done accurately.

$$F_s = \sum_{k=1}^{K} W_k * I_{enh} \qquad (10)$$

Equation 10 W_k Convolution kernel at scale k, F_s Multi-scale feature map, and, K Number of scales. Bone structure and fine tumor details of the images are obtained by extracting at different spatial resolutions.

$$F_f = FD(F_s) \qquad (11)$$

Equation 11 F_f Fractal-enhanced feature map, $FD(\cdot)$ Fractal dimension operator. Fractal coded the complexities of textures and irregular patterns of the tumors.

$$F_{nl} = \sigma(F_f) \qquad (12)$$

Equation 12 σ Non-linear activation function (ReLU), F_{nl} Activated feature map. Introduces non-linearity to emphasize tumor characteristics of discrimination.

$$F_{att} = CA(F_{nl}) \qquad (13)$$

Equation 13 $CA(\cdot)$ Channel attention operator, F_{att} Fattention-refined feature map. Enhances tumor specific channel and discourages other background aspects that are irrelevant.

3.3.3. Segmentation using FAGAS-Net

FAGAS-Net is a segmentation framework to apply the higher features to finer segmentation of the tumor regions with the overlay segmentation technique and contour mapping technique. Here, the estimated binary segmentation mask [25] is superimposed on the average bone image that results into making it easy to find the boundary of the tumor as well as the interpretation is also very easy.

In the meantime, the contour boundary mapping [15] is used to follow the precise boundaries of the segmented tumor that also reveal the abnormalities of shape and the complicated morphologic characteristics. The network is driven by a fractal model and adaptive graph attention to long-range spatial dependencies and non-uniform tumor morphology, and on blurred edges and a change in intensity, unstable, and it is more stable to these two.

Focus of attention mechanism is applied to streamline the overlay and the overlay produced contour representations to result in accurate mask-based segmentation which allows the overlay to give plausible results in tumor delineation, quantitative analysis and further solid clinical decision making.

$$G = (V, E),\ V = \{F_f^i\} \qquad (14)$$

Tianjin Daxue Xuebao (Ziran Kexue yu Gongcheng Jishu Ban)/
Journal of Tianjin University Science and Technology
ISSN (Online):0493-2137
E-Publication: Online Open Access
Vol: 59 Issue: 04:2026
DOI: 10.5281/zenodo.19495381

Equation 14 G Representation Grammar, V the nodes of which are feature vectors and E edges are spatial relationships of nodes. F_f^i Feature at pixel/region i. Transforms the image properties into a graph to denote the spatial and contextual relation.

$$\alpha_{ij} = \frac{\exp(Leaky\ ReLU(a^T[Wh_i \| Wh_j]))}{\sum_{k\epsilon\mathcal{N}_i}\exp(\cdot)} \quad (15)$$

Equation 15 α_{ij} Coefficients of attention between node i and node j, h_i, h_j Vector of node features, W Matrix of trainable weights, a Attention weight vectors, $\mathcal{N}_i$ Neighborhood of node i, ‖ Concatenation. Boosts the weighting of tumor relevant regions and inactivation of the background irrelevant nodes.

$$h_i' = \sigma\left(\sum_{j\epsilon\mathcal{N}_i}\alpha_{ij}Wh_j\right) \quad (16)$$

Equation 16 h_i', Unchanged node feature, σ Activation function, α_{ij} Clustering of information around to optimize features in order to represent a tumor boundary.

$$M = Softmax(W_s h') \quad (17)$$

Equation 17 M Predicted segmentation mask, W_s Segmentation classifier weights, h' Final node features. Produces a pixel, which is likely to be a tumor or non-tumor to distinguish the tumor and non-tumor regions accurately.

$$M_b = \mathbb{I}(M > \tau) \quad (18)$$

Equation 18 M_b Binary segmentation mask, τ Threshold value, $\mathbb{I}(\cdot)$ Indicator function, Converts probability map to final binary tumor segmentation mask.

Algorithm: Using Fractal–Adaptive Graph Attention Segmentation Network (FAGAS-Net)

```
Input: I      // Original medical image
// Step 1: Normalization & Enhancement
function NormalizeEnhance(I):
    Compute mean and standard deviation of I
    Standardize pixel intensities to reduce brightness variation
    Apply contrast enhancement to highlight tumor regions
    Scale intensities to a fixed range
    Apply CLAHE for local contrast improvement
    return enhanced image I_enh
// Step 2: Feature Enhancement
function FeatureEnhancement(I_enh):
    Extract multi-scale features using convolution
```

Tianjin Daxue Xuebao (Ziran Kexue yu Gongcheng Jishu Ban)/
Journal of Tianjin University Science and Technology
ISSN (Online):0493-2137
E-Publication: Online Open Access
Vol: 59 Issue: 04:2026
DOI: 10.5281/zenodo.19495381

```
    Enhance features with fractal-based representation
    Apply non-linear activation (e.g., ReLU)
    Refine features using channel attention
    return enhanced feature map F_att
// Step 3: Segmentation using FAGAS-Net with Overlay and Contour Mapping
function GraphAttentionSegmentation(F_att):
    Convert feature map F_att into a graph structure G(V, E)
    Compute adaptive attention weights between neighboring nodes
    Aggregate neighborhood information to refine node features
    Generate pixel-wise segmentation probability map P_seg
    Apply threshold τ to obtain binary tumor mask M_b
    // Overlay Segmentation
    Overlay tumor mask M_b on original image I_norm
       // Contour (Boundary) Mapping
    Extract boundary pixels from M_b
    Map tumor contours onto I_norm
    Generate contour-mapped image I_contour
    return M_b, I_overlay, I_contour
// Step 4: FAGAS-Net Pipeline
function FAGAS_Net(I):
    I_enh = NormalizeEnhance(I)            // Step 1
    F_att = FeatureEnhancement(I_enh)      // Step 2
    M_b = GraphAttentionSegmentation(F_att)  // Step 3
    return M_b
// Execute Algorithm
M_b = FAGAS_Net(I)
Output: M_b   // Binary tumor segmentation mask
```

The FAGAS-Net pseudo code describes a three step workflow of bone tumor segmentation. The input image is first normalized and contrast and noise reduced. Second, the combination of multi-scale and fractal-based enhancement of features and channel attention captures discriminative tumor features. Lastly, adaptive graph attention

Tianjin Daxue Xuebao (Ziran Kexue yu Gongcheng Jishu Ban)/
Journal of Tianjin University Science and Technology
ISSN (Online):0493-2137
E-Publication: Online Open Access
Vol: 59 Issue: 04:2026
DOI: 10.5281/zenodo.19495381

is used to process the features to come up with a probability map, which is thresholded to produce the final binary tumor segmentation mask.

4. RESULT AND DISCUSSION

The result of the proposed FAGAS-Net is a segmentation framework.The Quantitative and qualitative results are presented to assess the advancements in the quality of images and structural details and localization of tumor. Comparative tests in regard to state of the art models indicate the efficiency of proposed approach in producing accurate and reliable results of segmentation.

4.1 Normalization

The image enhancement phase used before the tumor segmentation stage is explained with the emphasis on the histopathological image denoising and normalization. Noise has to be suppressed and the variability in staining and the preservation of important tissue morphology have to be prevented by proper denoising in order to extract the necessary feature accurately. The qualitative and quantitative findings reveal that the proposed improvement plan enhances the image consistency and structural clarity massively, thus facilitating the credible downstream segmentation.

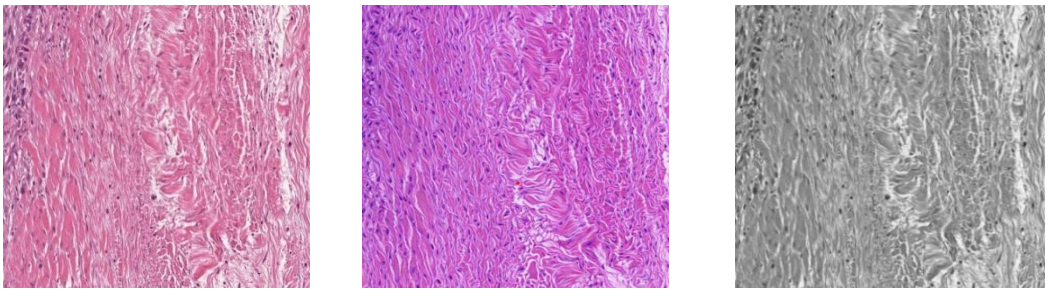

(a) Input Image **(b)Denoised Image** **(b)Normalized Image**

Figure 3: Histopathological Image Denoising and normalization

Figure 3 represents the most significant Denoising processes that are used to pre process the histopathological image prior to segmentation. Figure (a) is the initial input image that is noisy and has color variation. Figure (b) shows the denoised image in which the noise gets minimized without affecting the morphology of the tissue. Figure (c) plots the normalized image, the intensities are normalized and thus the features become easily consistent in the downstream analysis and segmentation.

Table 2: Metrics of Quantitative Image Enhancement

Metric	Result
Mean Intensity	0.0012
Standard Deviation	0.987
Contrast Improvement Index	1.68
Entropy	7.24

Tianjin Daxue Xuebao (Ziran Kexue yu Gongcheng Jishu Ban)/
Journal of Tianjin University Science and Technology
ISSN (Online):0493-2137
E-Publication: Online Open Access
Vol: 59 Issue: 04:2026
DOI: 10.5281/zenodo.19495381

Table 2 gives a summary of the quantitative assessment of the improved medical image following preprocessing. Mean Intensity measures the general balance in the brightness and Standard Deviation signifies better intensity distribution and contrast. The Contrast Improvement Index (CII) indicates that structural details are successfully improved and the Entropy value is also high to prove that when there are some structural details, richer texture information can be preserved after enhancement.

4.2 Feature Enhancement

The effectiveness of the proposed enhancement strategy is compared by means of the feature-enhanced bone tumor images presented in this section. Visual and quantitative evaluations are conducted to illustrate the changes in the contrast, structural details, and edge clarity. Such improvements are essential in order to increase the accuracy of the following tasks including the segmentation and detection of tumors.

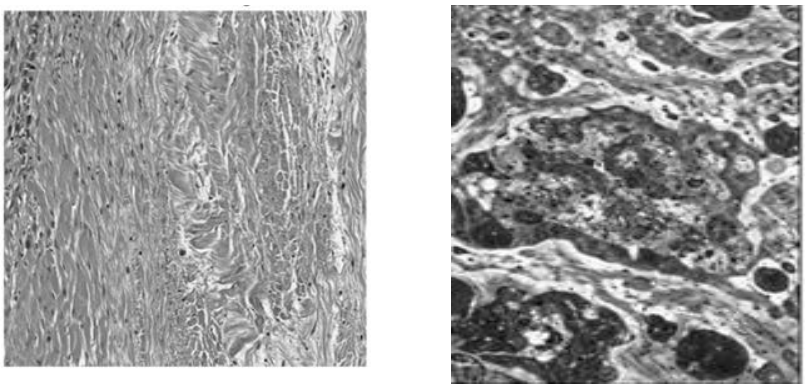

(a) Normalization input Image **(b) Feature Enhancement Image**

Figure 4: Comparison of Enhanced and Feature Image

Figure 4 outlines the dissimilarity between the original normalized photograph and the feature-enhanced photograph. The raw intensity distribution is presented by the image Normalization input (a), whereas the image feature-enhanced (b) demonstrates fine structural components, enhances contrast, and sharpens the edges. The improvement enables more efficient visualization of tissue structures and thus is more appropriate in further analysis (i.e. segmentation or tumor detection).

Table 3: Comparison of Metrics of Feature Enhancement

Metric	Original	Feature-Enhanced
Mean Intensity	0.0021	0.0015
Standard Deviation	0.986	1.025
Entropy	6.92	7.45
Contrast Improvement Index (CII)	1.00	1.52
Edge Preservation Index	0.76	0.88
Fractal Dimension	1.42	1.68
Contrast-to-Noise Ratio (CNR)	1.25	2.10

Tianjin Daxue Xuebao (Ziran Kexue yu Gongcheng Jishu Ban)/
Journal of Tianjin University Science and Technology
ISSN (Online):0493-2137
E-Publication: Online Open Access
Vol: 59 Issue: 04:2026
DOI: 10.5281/zenodo.19495381

Table 3 shows the important quantitative measures between the original and feature enhanced images. Measures that show improvement on image quality include Mean Intensity, Standard Deviation, Entropy, Contrast Improvement Index (CII), Edge Preservation Index, Fractal Dimension and Contrast-to-Noise Ratio (CNR). The result of the feature-enhanced image is increased values on entropy, CII, edge preservation, fractal dimension, and CNR which means that there is improved contrast, sharper edges and more information on the structure than in the original image.

4.3 Segmentation Result

The section includes the qualitative and quantitative analysis of the proposed FAGAS-Net regarding tumor segmentation. The visualizations at multiple stages depict how well features enhancement is done to enhance region localization and boundary demarcation. The comparison of the performance based on the standard segmentation metrics proves the superiority of FAGAS-Net in comparison with the existing state-of-the-art models.

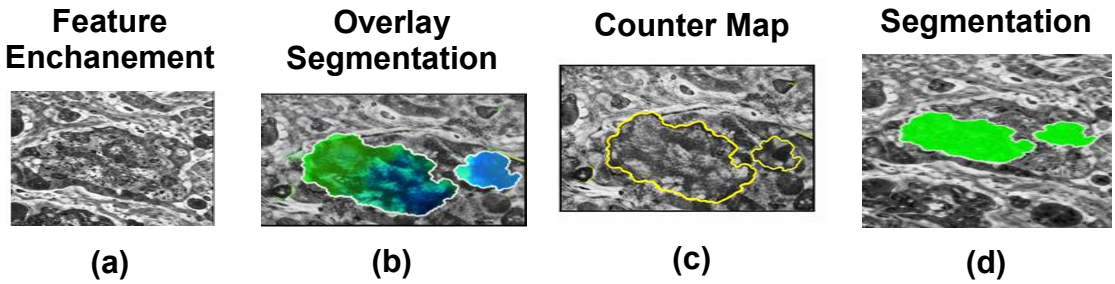

Figure 5: Segmentation at Multiple Stages Visualization

Figure 5 illustrates the full segmentation process beginning with the image that contains the features enhanced (a) and the end result of being a segmented image (d). The overlay segmentation (b) is a color-coded masks visualization to depict various tumor areas and the contour map (c) is used to identify the exact boundaries of the segmented areas. The last segmentation image (d) depicts the existence of the tumor regions in a distinct manner, indicating the usefulness of the proposed approach in the correct localization and delineation of the target structures.

Table 4: Comparison of the performance of segmentation

Algorithm	Dice Similarity Coefficient (DSC)	Jaccard Index (JI)	Precision	Recall	Hausdorff Distance (HD) (mm)
ResU-Net [25]	0.90	0.82	0.91	0.89	3.4
Dense U-Net [26]	0.89	0.81	0.90	0.88	3.6
Attention U-Net [27]	0.88	0.80	0.89	0.87	3.8
SegNet [28]	0.87	0.78	0.88	0.85	4.0
DeepLabV3+ [29]	0.86	0.77	0.87	0.84	4.2
FCN (Fully Convolutional Network) [30]	0.85	0.75	0.86	0.83	4.5
Proposed Algorithm (FAGAS-Net)	0.978	0.973	0.969	0.963	3.2

Table 4 presents a comparison of the performance of seven algorithms in segmentation based on five major measures, including Dice Similarity Coefficient (DSC), Jaccard Index

Tianjin Daxue Xuebao (Ziran Kexue yu Gongcheng Jishu Ban)/
Journal of Tianjin University Science and Technology
ISSN (Online):0493-2137
E-Publication: Online Open Access
Vol: 59 Issue: 04:2026
DOI: 10.5281/zenodo.19495381

(JI), Precision, Recall, and Hausdorff Distance (HD). The proposed FAGAS-Net demonstrates the highest level of DSC (0.978) and competitive values in other metrics, which means that it is more accurate and precise in defining boundaries during tumor segmentation than the current ones, such as ResU-Net, Dense U-Net, and Attention U-Net. In general, the table indicates that FAGAS-Net is more effective to provide more accurate and reliable segmentation results.

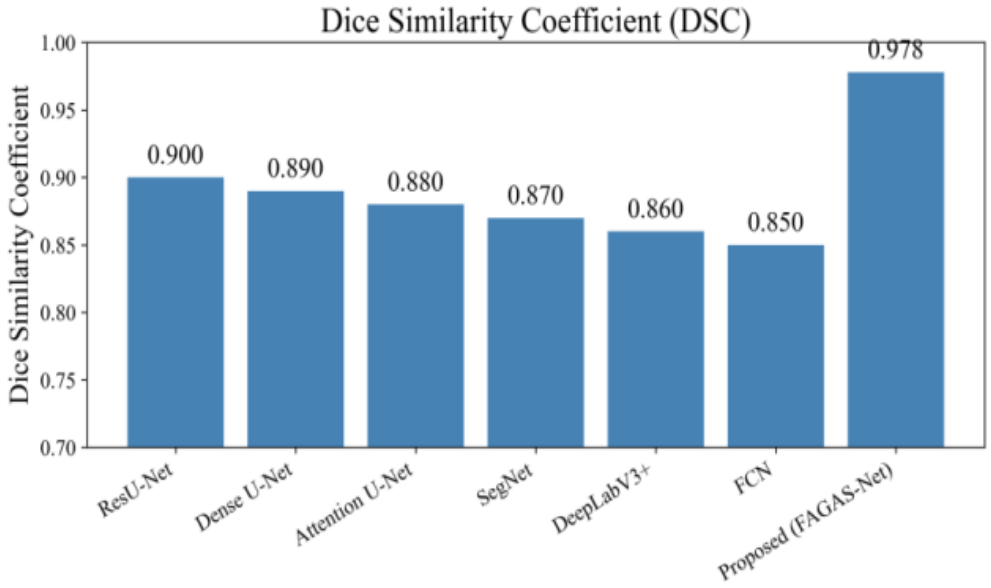

Figure 6: Dice Similarity Coefficient (DSC) comparison Chart

Figure 6 shows Dice Similarity Coefficient attained by various segmentation algorithms. The FAGAS-Net proposed is much more effective than the current procedures, meaning that the prediction of tumor regions and ground-truth annotations have better overlap.

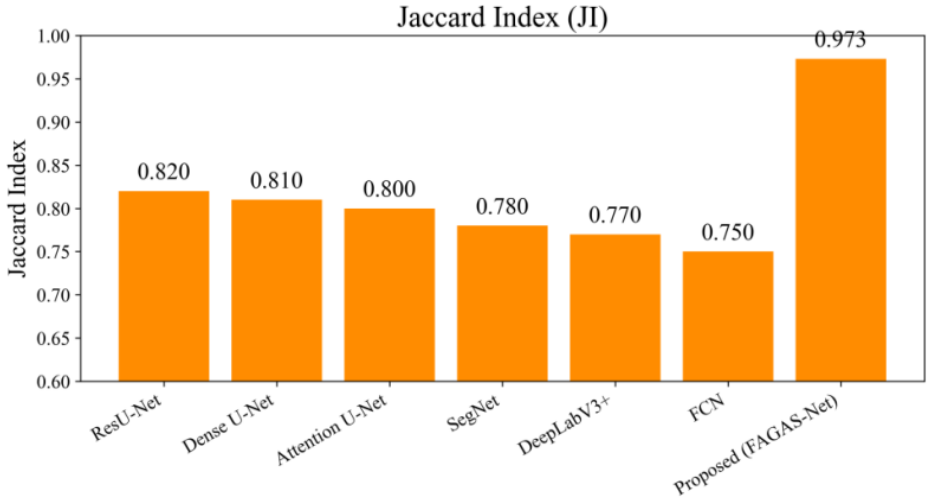

Figure 7: Jaccard Index (JI) of comparison

Tianjin Daxue Xuebao (Ziran Kexue yu Gongcheng Jishu Ban)/
Journal of Tianjin University Science and Technology
ISSN (Online):0493-2137
E-Publication: Online Open Access
Vol: 59 Issue: 04:2026
DOI: 10.5281/zenodo.19495381

Figure 7 bar chart shows all the evaluated models values of the Jaccard Index. The increased JI as achieved by FAGAS-Net shows that it is superior in capturing the tumor regions more consistently with few false overlaps.

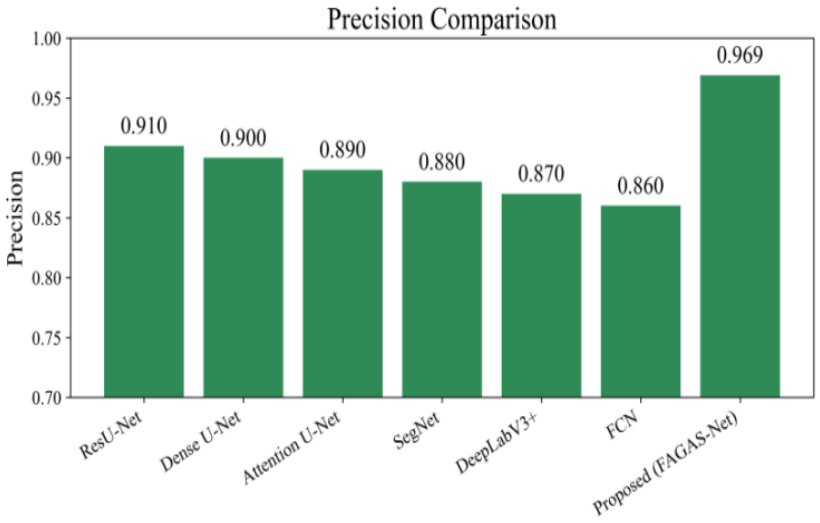

Figure 8: Precision comparison

Figure 8 is a comparison of the precision scores of different segmentation networks. The proposed technique is the most precise, which means that it is effective to minimize false-positive tumor detection.

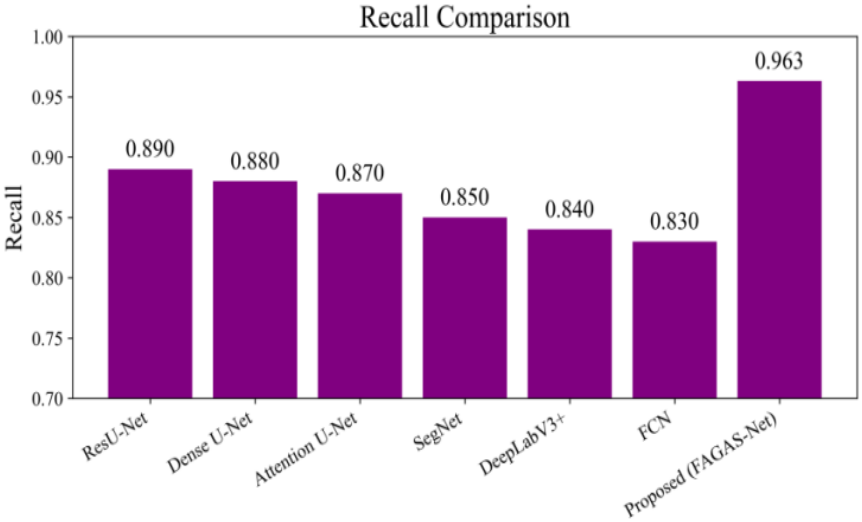

Figure 9: Recall comparison

Figure 9 bar chart indicates the performance of various algorithms in terms of recall. FAGAS-Net can achieve better recall which validates its strength in the correct recognition of most tumor pixels.

Tianjin Daxue Xuebao (Ziran Kexue yu Gongcheng Jishu Ban)/
Journal of Tianjin University Science and Technology
ISSN (Online):0493-2137
E-Publication: Online Open Access
Vol: 59 Issue: 04:2026
DOI: 10.5281/zenodo.19495381

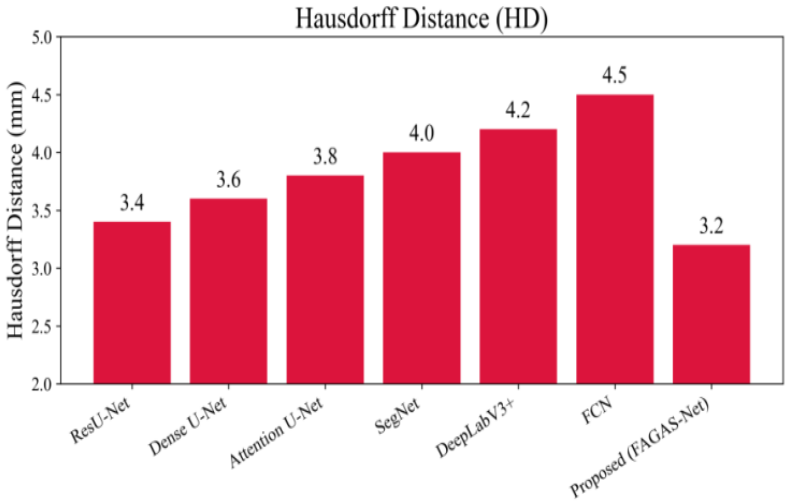

Figure 10: Comparison of Hausdorff Distance (HD)

Figure 10 shows the Hausdorff Distance of every of the segmentation methods. The low value of HD of FAGAS-Net shows a better alignment of boundaries and a better localization of tumor boundaries.

5. CONCLUSION

FAGAS-Net used to precisely delineate tumor boundaries of bone sarcoma by using histopathological images. The multi-stage denoising, enhancements of features and adaptive attention of the graph made the framework successfully handle the issues of heterogeneous tumor textures, weak contrast and irregular edges of the lesions. Multi-scale and fractal-based feature extraction ensured that both global structural images and fine tumor images were captured and the attention-directed graph modeling focused on tumor-specific images and meanwhile removed the background noise. The experimental findings showed that FAGAS-Net was superior to the current state-of-the-art. Evaluation of the visual assessment revealed the accurate localization of tumors and well-defined borders, which can be used to make reliable medical decisions. The proposed solution creates a strong, universalized system of automated bone sarcoma segmentation. The next step in the work will be creating FAGAS-Net to be extended to multimodal imaging data and provide real-time segmentation features to improve medical usefulness and surgical planning.

Reference

1) Vezakis, I. A., Lambrou, G. I., & Matsopoulos, G. K. (2023). Deep learning approaches to bone sarcoma diagnosis and classification: A comparative methodological approach. Cancers, 15(8), 2290. https://doi.org/10.3390/cancers15082290

2) Fakieh, B., Al-Ghamdi, A. S. A. M., & Ragab, M. (2022, June). Optimal deep stacked sparse autoencoder based bone sarcoma detection and classification model. In Healthcare (Vol. 10, No. 6, p. 1040). MDPI. https://doi.org/10.3390/healthcare10061040

Tianjin Daxue Xuebao (Ziran Kexue yu Gongcheng Jishu Ban)/
Journal of Tianjin University Science and Technology
ISSN (Online):0493-2137
E-Publication: Online Open Access
Vol: 59 Issue: 04:2026
DOI: 10.5281/zenodo.19495381

3) Gawade, S., Bhansali, A., Patil, K., & Shaikh, D. (2023). Application of the convolutional neural networks and supervised deep-learning methods for bone sarcoma bone cancer detection. Healthcare analytics, 3, 100153. https://doi.org/10.1016/j.health.2023.100153

4) Aziz, M. T., Mahmud, S. H., Elahe, M. F., Jahan, H., Rahman, M. H., Nandi, D., ... & Moni, M. A. (2023). A novel hybrid approach for classifying bone sarcoma using deep feature extraction and multilayer perceptron. Diagnostics, 13(12), 2106. https://doi.org/10.3390/diagnostics13122106

5) Anand, D., Khalaf, O. I., Hajjej, F., Wong, W. K., Pan, S. H., & Chandra, G. R. (2023). Optimized Swarm Enabled Deep learning technique for bone tumor detection using Histopathological Image. SINERGI, 27(8), 451-466. https://doi.org/10.1016/j.jbo.2024.100644

6) Rao, B. D., & Madhavi, K. (2025). Enhancing bone cancer detection through optimized pre trained deep learning models and explainable AI using the bone sarcoma tumor assessment dataset. Scientific Reports, 15(1), 39104. https://doi.org/10.1038/s41598-025-26051-8

7) Prabakaran, S., & Praveena, S. M. (2025). Improved gated recurrent unit-based bone sarcoma prediction on histology images: a meta-heuristic-oriented optimization concept. Scientific Reports, 15(1), 11179. https://doi.org/10.1038/s41598-025-85149-1

8) Walid, M. A. A., Mollick, S., Shill, P. C., Baowaly, M. K., Islam, M. R., Ahamad, M. M., ... & Samad, M. A. (2023). Adapted deep ensemble learning-based voting classifier for bone sarcoma cancer classification. Diagnostics, 13(19), 3155. https://doi.org/10.3390/diagnostics13193155

9) Vaiyapuri, T., Jothi, A., Narayanasamy, K., Kamatchi, K., Kadry, S., & Kim, J. (2022). Design of a honey badger optimization algorithm with a deep transfer learning-based bone sarcoma classification model. Cancers, 14(24), 6066. https://doi.org/10.3390/cancers14246066

10) Gou, F., Liu, J., Zhu, J., & Wu, J. (2022, October). A multimodal auxiliary classification system for bone sarcoma histopathological images based on deep active learning. In Healthcare (Vol. 10, No. 11, p. 2189). MDPI. https://doi.org/10.3390/healthcare10112189

11) Nasir, M. U., Khan, S., Mehmood, S., Khan, M. A., Rahman, A. U., & Hwang, S. O. (2022). IoMT-based bone sarcoma cancer detection in histopathology images using transfer learning empowered with blockchain, fog computing, and edge computing. Sensors, 22(14), 5444. https://doi.org/10.3390/s22145444

12) Tang, H., Sun, N., & Shen, S. (2021). Improving generalization of deep learning models for diagnostic pathology by increasing variability in training data: experiments on bone sarcoma subtypes. Journal of Pathology Informatics, 12(1), 30.https://doi.org/10.4103/jpi.jpi_78_20

13) Vaiyapuri, T., Dutta, A. K., Punithavathi, I. H., Duraipandy, P., Alotaibi, S. S., Alsolai, H., ... & Mahgoub, H. (2022, April). Intelligent deep-learning-enabled decision-making medical system for pancreatic tumor classification on CT images. In Healthcare (Vol. 10, No. 4, p. 677). MDPI.https://doi.org/10.3390/healthcare10040677

14) Kotei, E., & Thirunavukarasu, R. (2022, November). Ensemble technique coupled with deep transfer learning framework for automatic detection of tuberculosis from chest X-ray radiographs. In Healthcare (Vol. 10, No. 11, p. 2335). MDPI.https://doi.org/10.3390/healthcare10112335

15) Ye, Z., Kumar, Y. J., Song, F., Li, G., & Zhang, S. (2023). Bi-dcnet: Bilateral network with dilated convolutions for left ventricle segmentation. Life, 13(4), 1040.https://doi.org/10.3390/life13041040

16) Georgeanu, V. A., Mămuleanu, M., Ghiea, S., & Selișteanu, D. (2022). Malignant bone tumors diagnosis using magnetic resonance imaging based on deep learning algorithms. Medicina, 58(5), 636.https://doi.org/10.3390/medicina58050636

Tianjin Daxue Xuebao (Ziran Kexue yu Gongcheng Jishu Ban)/
Journal of Tianjin University Science and Technology
ISSN (Online):0493-2137
E-Publication: Online Open Access
Vol: 59 Issue: 04:2026
DOI: 10.5281/zenodo.19495381

17) Breden, S., Hinterwimmer, F., Consalvo, S., Neumann, J., Knebel, C., von Eisenhart-Rothe, R., ... & Lenze, U. (2023). Deep learning-based detection of bone tumors around the knee in X-rays of children. Journal of Clinical Medicine, 12(18), 5960.https://doi.org/10.3390/jcm12185960

18) Kim, J., Jeong, S. Y., Kim, B. C., Byun, B. H., Lim, I., Kong, C. B., ... & Woo, S. K. (2021). Prediction of neoadjuvant chemotherapy response in bone sarcoma using convolutional neural network of tumor center 18F-FDG PET images. Diagnostics, 11(11), 1976.https://doi.org/10.3390/diagnostics11111976

19) Mămuleanu, M., Urhuț, C. M., Săndulescu, L. D., Kamal, C., Pătrașcu, A. M., Ionescu, A. G., ... & Streba, C. T. (2022). Deep learning algorithms in the automatic segmentation of liver lesions in ultrasound investigations. Life, 12(11), 1877.https://doi.org/10.3390/life12111877

20) Zhao, Y., Guo, Q., Zhang, Y., Zheng, J., Yang, Y., Du, X., ... & Zhang, S. (2023). Application of deep learning for prediction of Alzheimer's disease in PET/MR imaging. Bioengineering, 10(10), 1120.https://doi.org/10.3390/bioengineering10101120

21) Pati, A., Parhi, M., Pattanayak, B. K., Sahu, B., & Khasim, S. (2023). CanDiag: Fog empowered transfer deep learning based approach for cancer diagnosis. Designs, 7(3), 57. https://doi.org/10.3390/designs7030057

22) Chen, S., Peng, Y., Liu, Y., Wang, P., & Liu, T. (2025). Enhancing YOLOv11 with Large Kernel Attention and Multi-Scale Fusion for Accurate Small and Multi-Lesion Bone Tumor Detection in Radiographs. Diagnostics, 15(16), 1988. https://doi.org/10.3390/diagnostics15161988

23) Karabağ, C., Ortega-Ruíz, M. A., & Reyes-Aldasoro, C. C. (2023). Impact of training data, ground truth and shape variability in the deep learning-based semantic segmentation of HeLa cells observed with electron microscopy. Journal of Imaging, 9(3), 59.https://doi.org/10.3390/jimaging9030059

24) Wang, L., Yu, L., Zhu, J., Tang, H., Gou, F., & Wu, J. (2022, August). Auxiliary segmentation method of bone sarcoma in MRI images based on denoising and local enhancement. In Healthcare (Vol. 10, No. 8, p. 1468). MDPI. https://doi.org/10.3390/healthcare10081468

25) Sabir, M. W., Khan, Z., Saad, N. M., Khan, D. M., Al-Khasawneh, M. A., Perveen, K., ... & Azhar Ali, S. S. (2022). Segmentation of liver tumor in CT scan using ResU-Net. Applied Sciences, 12(17), 8650. https://doi.org/10.3390/app12178650

26) Wang, K., Han, Y., Ye, Y., Chen, Y., Zhu, D., Huang, Y., ... & Huang, J. (2025). Mixed reality infrastructure based on deep learning medical image segmentation and 3D visualization for bone tumors using DCU-Net. Journal of Bone Oncology, 50, 100654. https://doi.org/10.1016/j.jbo.2024.100654

27) Brunese, M. C., Rocca, A., Santone, A., Cesarelli, M., Brunese, L., & Mercaldo, F. (2025). Explainable and robust deep learning for liver segmentation through U-net network. Diagnostics, 15(7), 878. https://doi.org/10.3390/diagnostics15070878

28) Della Reasa Valiaveetil, K. T. (2025). Leukemia detection using SegNet and faster region-based convolutional neural network. International Journal of Electrical and Computer Engineering (IJECE), 15(3), 3028-3038. DOI: 10.11591/ijece.v15i3.pp3028-3038

29) Zhou, W., Chen, Y., Liu, D., He, H., Zhong, L., & Zhong, Y. (2025). Intelligent Layout Segmentation and Classification of Packaging Labels Using Enhanced DeepLabv3+ with Multi-Scale Feature Optimization. https://doi.org/10.21203/rs.3.rs-8361346/v1

30) Lu, N. H., Wang, C. Y., Liu, K. Y., Huang, Y. H., & Chen, T. B. (2025). AI-Enhanced Deep Learning Framework for Pulmonary Embolism Detection in CT Angiography. Bioengineering, 12(10), 1055.https://doi.org/10.3390/bioengineering12101055